

PLOVDIV UNIVERSITY "PAISII HILENDARSKI"



FACULTY OF PHYSICS AND TECHNOLOGY

DEPARTMENT OF ELECTRONICS, COMMUNICATIONS AND INFORMATION TECHNOLOGY"

M. Eng. Anatoliy Rosenov Parushev,

AUTOMATION OF A LABORATORY FOR ECO-ENERGY TECHNOLOGIES

ABSTRACT

of a dissertation for the acquisition of an educational and scientific degree "DOCTOR"

Field of higher education:

5. Technical sciences

Professional field:

5.3. "Communication and computer technology"

Doctoral program:

"Automation of areas of the intangible sphere (medicine, education, science, administrative activities, etc.)"

Scientific supervisor:

Prof.Dr. Eng. Rumen Kostadinov Popov

The dissertation is 224 pages long, including 81 figures, 19 tables, arranged in an introduction, 5 chapters, general conclusions, scientific and applied contributions, a list of used designations and abbreviations, a list of the author's publications. The list of cited literature includes 139 titles.

The designations of the formulas, figures and tables in the abstract coincide with those in the dissertation at a meeting of the scientific jury.

The dissertation work was discussed and directed for defense at a meeting of the extended department council of the department "ELECTRONICS, COMMUNICATIONS AND INFORMATION TECHNOLOGIES" at the UNIVERSITY OF PLOVDIV "PAISII HILENDARSKI" on 15.10.2025, Protocol No. 81.

The dissertation defense will take place on 05.12.2025 at

The materials for the doctoral defense are available to those interested in the office of the Faculty of Physics and Technology at the "PAISII HILENDARSKI" UNIVERSITY OF PLOVDIV, room 214.

Scientific jury: Prof. Dr. Rositsa Zhelyazkova Doneva

Prof. Dr. Eng. Atanaska Dimitrova Bosakova-Ardenska

Prof. Dr. Eng. Seville Aptula Ahmed-Shieva

Assoc. Prof. Dr. Eng. Sotir Ivanov Sotirov

Assoc. Prof. Dr. Eng. Vladimira Krasteva Ganchovska

Author: M.Eng. Anatoly Rosenov Parushev

Title: AUTOMATION OF A LABORATORY FOR ECO-ENERGY TECHNOLOGIES

Circulation: 30 pcs.

GENERAL CHARACTERISTICS OF THE DISSERTATION

Relevance of the problem

In an era of global transformations in the energy sector and increasing digitalization of engineering systems, the need for sustainable, automated and accessible technological solutions is more tangible than ever. The pressure to transition to green energy and intelligent resource management is accompanied by the need to modernize education, research and engineering practice.

Laboratory automation is a modern response to these needs. Systems based on sensors, actuators, programmable controllers and software platforms allow precise control, flexible configuration and remote access to laboratory equipment.

The ability to work with real objects in real time – regardless of the user's geographical location – is key to building a new model of engineering training. In addition to the educational value, such systems also have research potential. They allow for the accumulation of empirical data, the conduct of a series of experiments with controlled parameters, as well as the repeatability and traceability of results – requirements characteristic of modern scientific methodology.

The combination of capabilities for automatic data collection, processing and visualization turns the laboratory not just into a place for demonstration, but into an active environment for discovering and validating new knowledge.

Building such systems requires an interdisciplinary approach, combining knowledge from electronics, communication technologies, programming, energy, and engineering pedagogy. This combination is necessary to create a functional, sustainable, and accessible system that can be integrated into both educational and applied scientific contexts.

In today's environment, when education is increasingly transitioning to hybrid or distance learning, the importance of automated remote access laboratories is increasing. They are becoming an alternative to classic laboratory classes, providing access to real equipment and processes via the Internet, without compromising the quality of education. Such solutions contribute to more equal access to technological resources, regardless of the physical location or financial capabilities of the educational institution.

This dissertation is motivated by the need to create a sustainable, scalable and functional laboratory system in the field of eco-energy technologies that meets modern requirements for automation, digitalization and open access.

Purpose of the dissertation:

The aim of this dissertation is the development, construction and experimental validation of an automated laboratory bench with remote control capabilities, intended for training and research of thermal processes. The system should be scalable, reliable and applicable in both educational and research environments.

Tasks to achieve the goal:

- 1. To analyze the existing state of the art in the field of tools and technologies for building automated laboratory systems suitable for conducting distance learning.
- 2. To design and implement a hardware architecture of a laboratory bench with the ability for remote control and real-time monitoring.
- 3. To develop a communication infrastructure based on industrial protocols (Modbus, TCP/IP) and modern IoT solutions.
- 4. To create and configure a software system for storing, visualizing, controlling, and analyzing experimental data using an environment such as Node-RED.
- 5. To create a methodology for measuring and analyzing velocity, mass flow rate and thermodynamic parameters of air flow in a closed duct.
- 6. To conduct experimental studies of the velocity and volumetric flow rate of air flow in a closed duct when varying the fan performance.
- 7. To determine the specific heat capacity, enthalpy and internal energy of the air flow under different operating modes.

Research methods and tools used:

The dissertation applies experimental methodologies for determining the velocity profile and air flow rate using a Pitot tube on an SR1162E stand, with control and remote access via Modbus RS-485/TCP/IP and visualization in Node-RED.

Implementation and practical applicability

The developed system provides a sustainable platform for distance learning and research, optimizes laboratory activities, reduces costs, and ensures equal access to real experiments and data.

Publications on the topic

The results of the dissertation work have been published in 6 scientific articles: 1 in the proceedings of the XXXIII International Scientific Conference Electronics ET 2024, indexed in Scopus, 5 in proceedings of international conferences INTED 2023 and ICERI 2022. All publications are co-authored with the scientific supervisor.

Scope and structure of the dissertation work

The dissertation is 224 pages long, including 81 figures, 19 tables, arranged in an introduction, 5 chapters, general conclusions, scientific and applied contributions, a list of abbreviations and notations used, a list of the author's publications. The list of cited literature includes 139 titles.

CONTENT OF THE DISSERTATION

CHAPTER 1. OVERVIEW OF LABORATORY AUTOMATION TOOLS IN THE FIELD OF ECO-ENERGY TECHNOLOGIES.

In chapter one of the dissertation, a literature review on the issue under consideration is conducted. An analysis of the current state and trends in the development of remote and virtual laboratories is presented. Figure 1 visualizes the block diagrams of a remote and virtual laboratory stand.

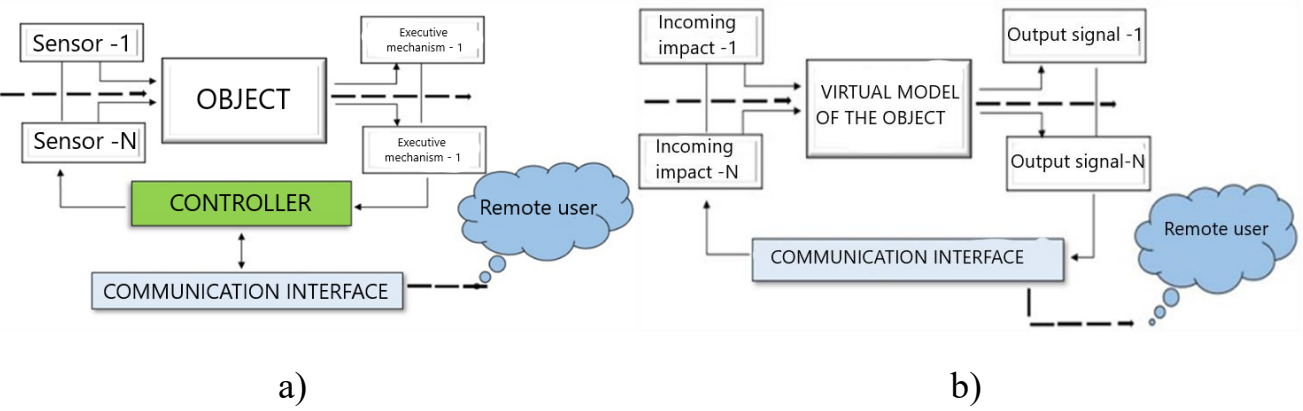


Figure 1.1 Generalized schemes of a remote a) and virtual b) laboratory stand

The features of the main architectural solutions are specified, with an emphasis on the hardware and software platforms that provide monitoring and control of processes. Systems based on programmable logic controllers (PLC) and specialized microcontrollers are examined in detail. A detailed analysis of the protocols and internal system interfaces for communication is made. Table 1.1 presents a comparative analysis between different software platforms.

Tubic 1.1 Computative unarysis of some software platforms							
Platform	Basic functionality	Applications	Integration	Security			
SCADA	Monitoring and control of industrial processes	Industrial sectors: energy, water supply	Integration with PLC, HMI, MES, etc.	Built-in mechanisms for protection against cyber attacks			
Energy management systems	Monitoring and management of energy resources and systems	Buildings, industrial sites, public buildings	Integration with sensors, accounting systems, etc.	Data and communications protection			
Internet of Things Platforms	Collection, processing and analysis of data from connected devices	Industry 4.0, smart cities, healthcare	Integration with various IoT devices	Data encryption and device identification			
Energy analysis software	Monitoring and analysis of energy consumption	Buildings, industrial facilities, renewable sources	Integration with accounting systems and sensors	Allow access and encrypt data			

Table 1.1 Comparative analysis of some software platforms

Platform	Basic functionality	Applications	Integration	Security
Remote monitoring and control systems	Monitoring and control of distributed systems	Energy installations, transmission networks, transport	Integration with sensors, PLCs, IoT devices	Access control and communication encryption

The limitations identified from the literature review are analyzed. To achieve the set goal, the tasks of the dissertation are defined. The relevance of the topic is emphasized, arising from the need to increase access to specialized equipment and reduce the costs of conducting experiments, which is in line with the EU policies for digitalization and green transformation.

The review found that the most adverse impact on the effectiveness of remote laboratories is the lack of integration between hardware and software, insufficient interactivity and limited opportunities for simulation of real processes. Particular attention is paid to compliance with security standards, as well as the use of modern methods and systems for visualization and remote control of experiments.

CHAPTER 2. RESEARCH METHODOLOGY

In chapter two of the dissertation, a methodology for conducting experimental studies is developed. It includes both the selection and configuration of real equipment, as well as the development of a suitable architecture for automation and remote access. The SR1162E heat transfer bench (Figure 2.1), used as the main experimental setup, is presented and its components are described.

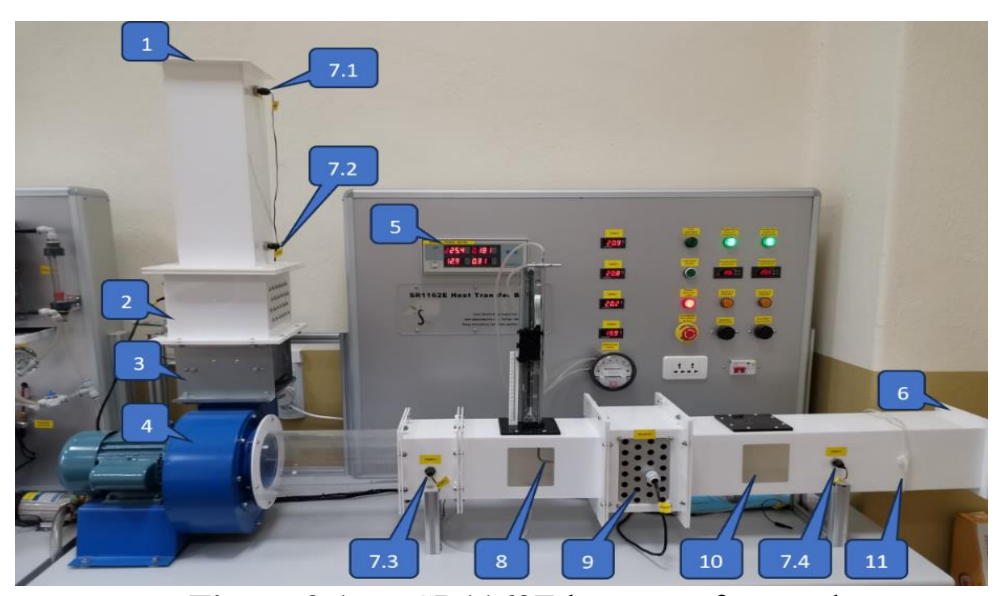


Figure 2.1 SR1162E heat transfer stand

For the needs of remote control, a block diagram for remote power control has been built (Figure 2.2), as well as a block diagram of an automated SR1162E stand (Figure 2.3), in which the individual functional modules are clearly distinguished - measuring sensors, control controller, communication interface and user access.

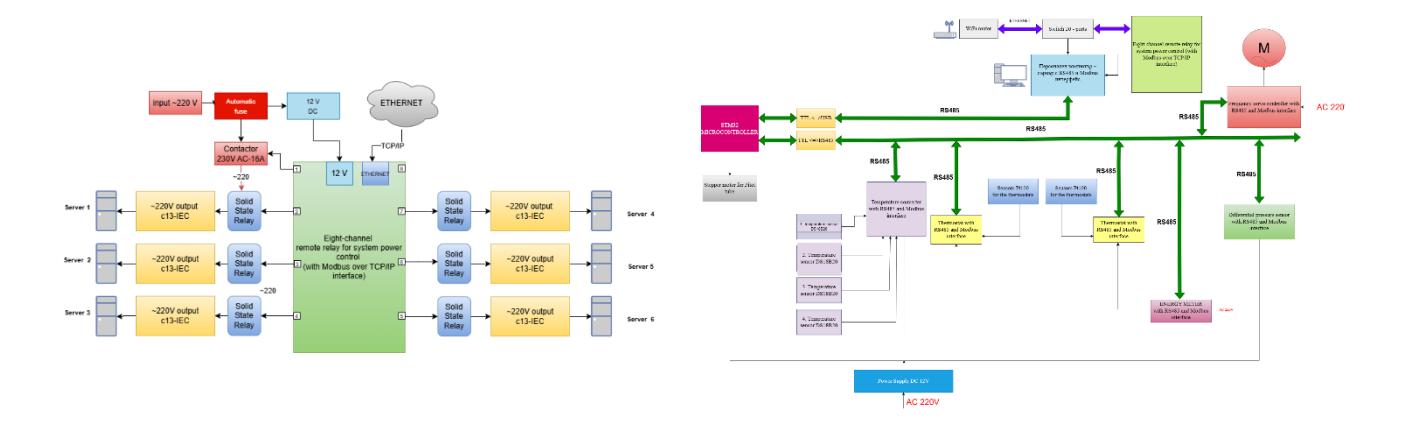


Figure 2.2 Block diagram of remote power control

Figure 2.3 Block diagram of an automated laboratory bench

Two methodologies are presented and described in detail. The first is related to the determination of the air flow velocity profile in a rectangular tube. The methods for measuring the velocity are presented in detail, and a block diagram of the experimental setup is implemented, presented in Figure 2.4.

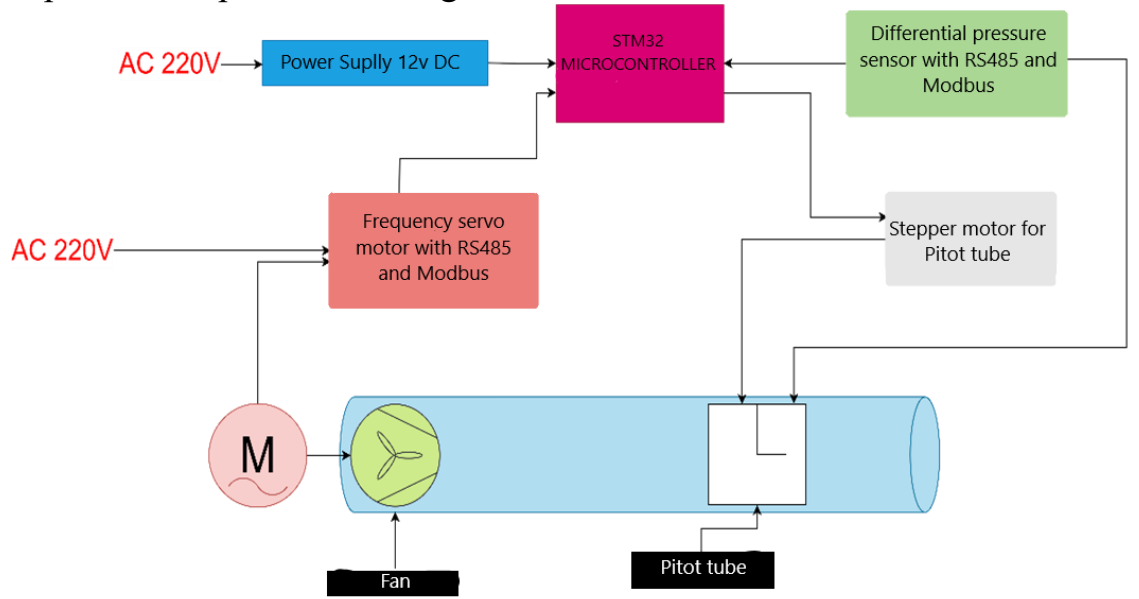


Figure 2.4 Block diagram of the experimental setup

The components of the system are presented step by step, while the formulas for determining the air density and volumetric flow rates for the relevant sections are analyzed and defined. The block diagram of the distribution of the sections for measuring the air flow is presented in Figure 2.5.

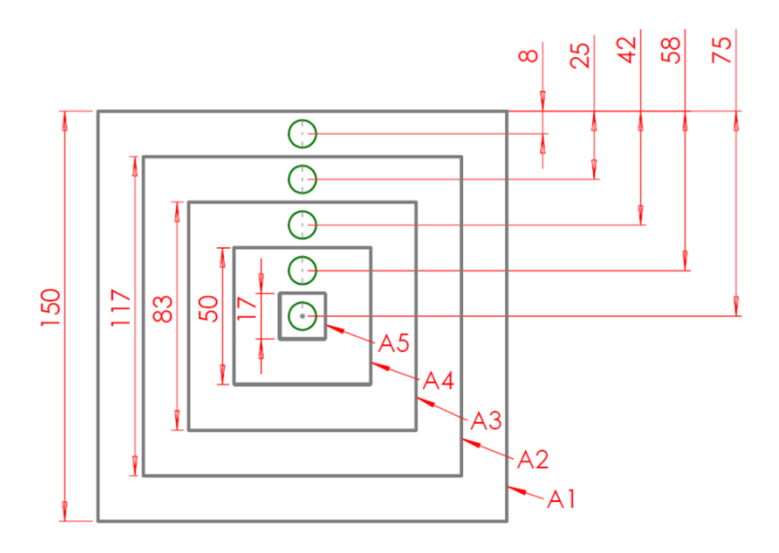


Figure 2.5 Airflow measurement cross-section distribution diagram

The second methodology is related to the determination of the specific heat capacity of air at constant pressure. It emphasizes the accuracy of measuring the mass flow rate and the temperature difference of the air flow, and the energy balance ensures a reliable calculation of the heat capacity.

An analysis of the methods used for remote access and control is made. The Modbus over TCP/IP interface is described and its data frame and architecture are discussed, presented in Figure 2.6.

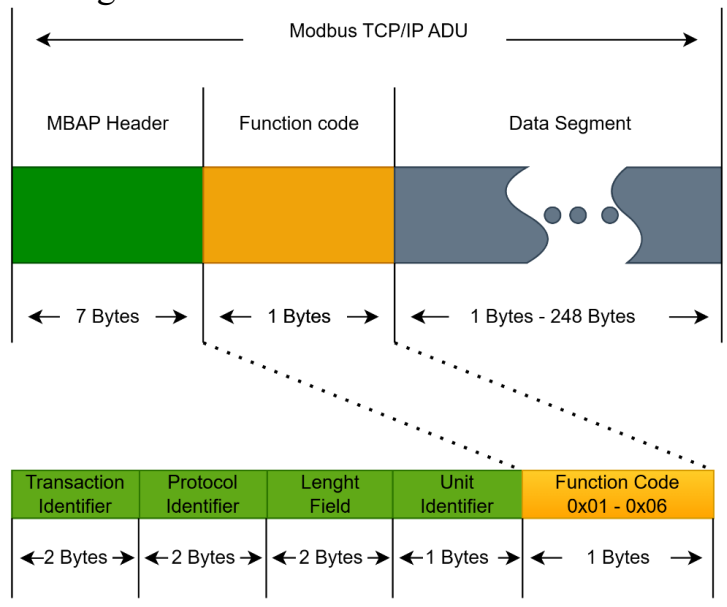


Figure 2.6 Modbus TCP/IP data frame

In conclusion, chapter two presents a comprehensive experimental methodology that combines a real laboratory stand and additional air flow study facilities, automation through programmable controllers and remote access. This creates prerequisites for effective study of thermal processes and validation of models used in virtual laboratory environments.

2.1 CONCLUSIONS OF CHAPTER 2

The research conducted in the second chapter shows that the SR1162E stand is a reliable and highly efficient platform for studying thermal processes, providing the necessary accuracy of measurements thanks to the built-in sensors and integrated control systems. The methods for measuring the velocity profile and airflow rate have proven

their precision and reliability, allowing the calculation of basic parameters of high engineering value. In addition, the study of remote access and the application of communication protocols and intelligent controllers has shown that the stand can be modernized and adapted to modern requirements, which makes it a valuable tool not only for training and scientific purposes, but also for real industrial applications.

CHAPTER 3. DEVELOPMENT OF AN AUTOMATED STAND WITH REMOTE ACCESS

Chapter three of the dissertation presents the development of an automated laboratory bench with the ability for remote control and monitoring. The structure of the bench is organized into separate subsystems, each of which is designed to perform specific functions and be integrated into the overall control architecture.

3.1 Remote power control system

For the purposes of the dissertation, a mock-up presented in Figure 3.1 was designed and implemented, providing remote switching on and off of the server(s), on which the main software product providing visual presentation of all necessary measurement data will be located. The developed system provides the ability for precise power control via Modbus commands, which are fed to the eight-channel remote power control relay.

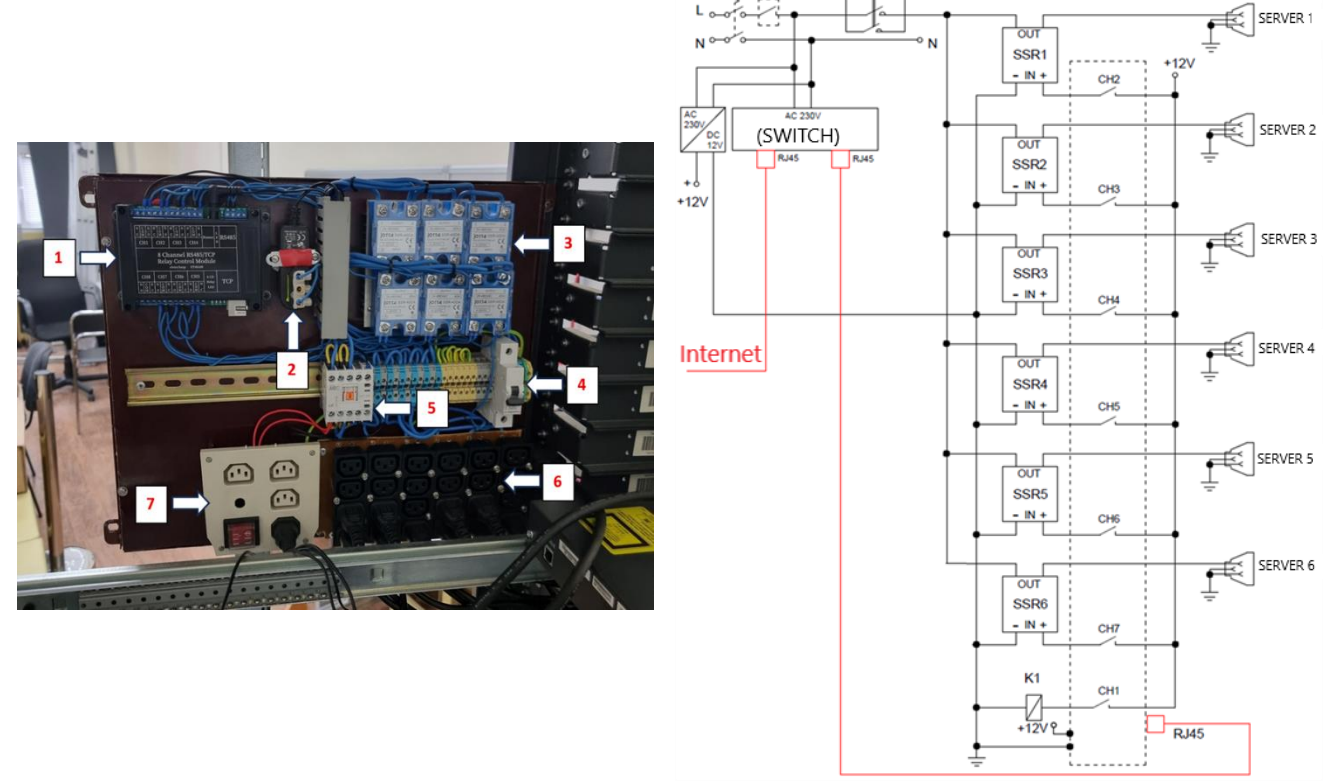


Figure 3.1 Construction and schematic diagram of the remote power control system: (1. Eight-channel remote power control relay; 2. 12 V DC power supply unit; 3. Solid-state relay; 4. Circuit breaker; 5. 230V AC 16A contactor; 6. Output power connectors (c13-IEC); 7. 230 V constant power supply)

3.2 Stand equipment

A. Ventilation system

The ventilation system of the bench is visualized in block diagram and through its main electrical diagram in Figure 3.2. It is designed to provide effective control of the air flow of the laboratory setup.

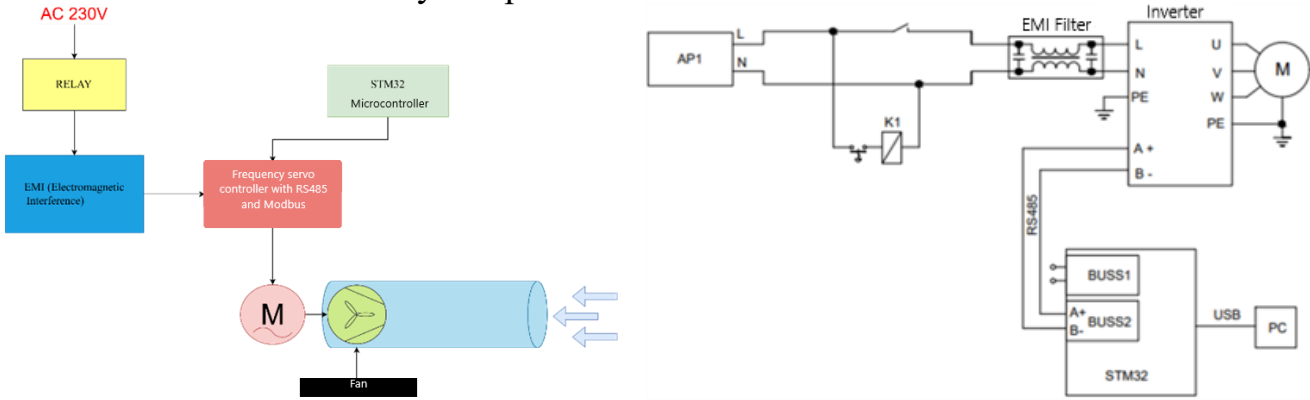


Figure 3.2 Block and principle electrical diagram of the ventilation system

The dissertation describes all the components of the system. Their characteristics are presented in tabular form, with special attention paid to the asynchronous electric motor and the frequency servo drive.

B. Airflow measurement system

The laboratory bench airflow measurement system and its schematic and electrical diagram are presented in Figure 3.3. It is designed to provide airflow control using a Pitot tube, with data being read and transmitted to the microcontroller via a differential pressure sensor with a Modbus RS485 interface.

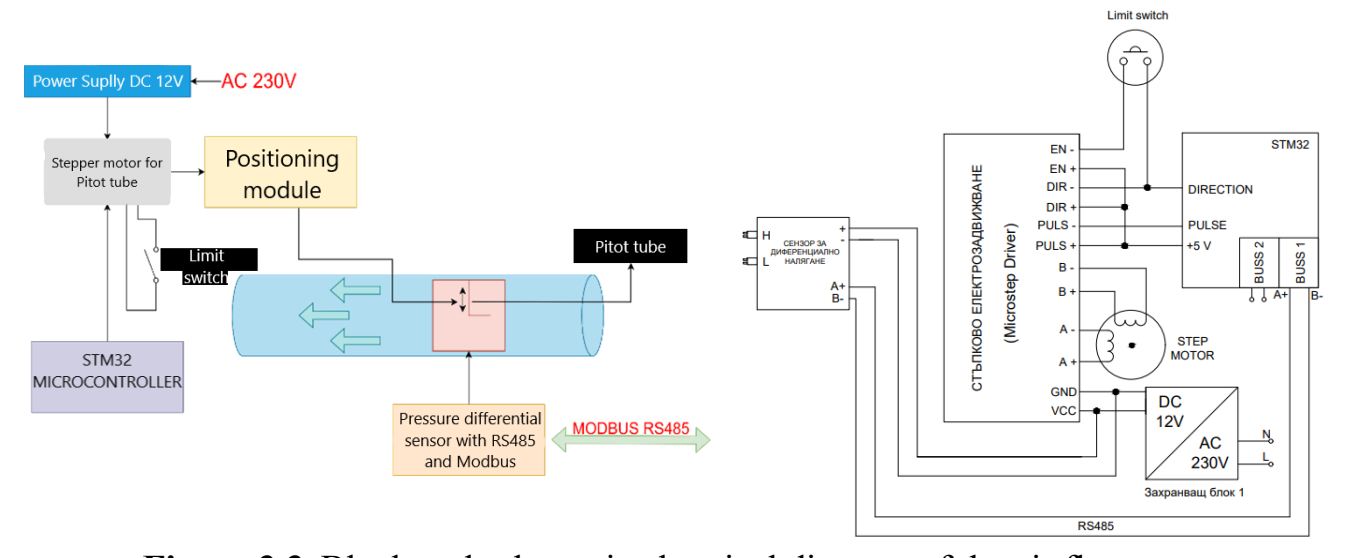


Figure 3.3 Block and schematic electrical diagram of the air flow measurement system

The components of the system were examined, and an analysis was made for the selection of specific hardware components. A 3D model was designed and printed on a Bambu Lab P1S 3D printer, its main function being to ensure smooth and controlled movement of the Pitot tube at predetermined points.

C. Temperature control system and energy consumption

The system is presented in block form in Figure 3.4 and is designed for precise temperature control and energy monitoring for the purpose of experimental study of heat transfer processes in the laboratory bench. The control and data collection is carried out by an STM32 microcontroller, and the communication between the individual elements is implemented via an RS485 bus with Modbus protocol.

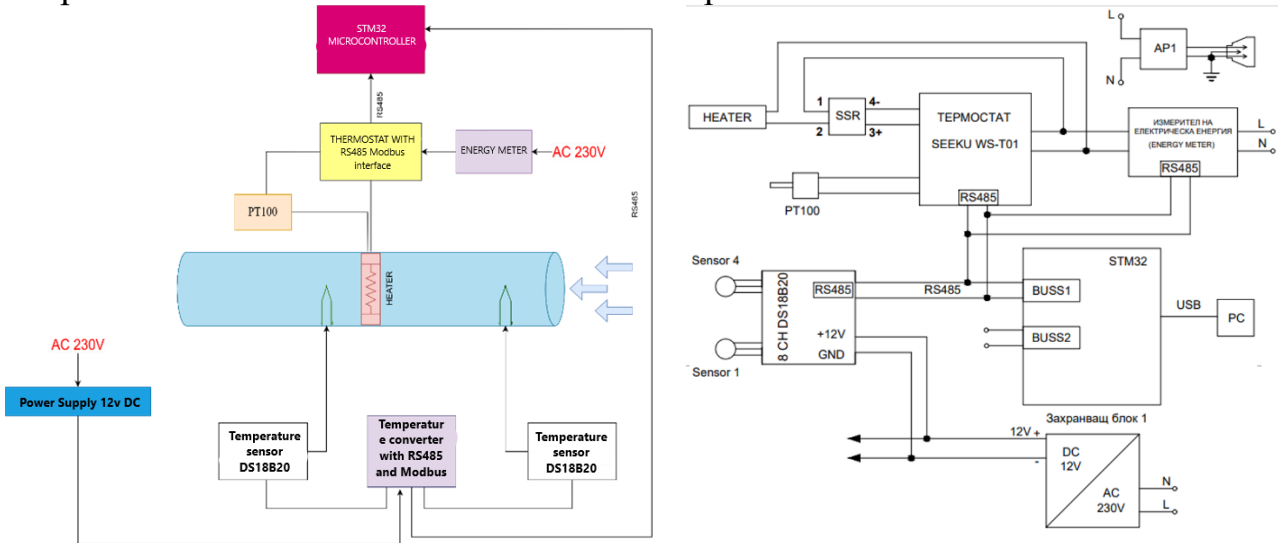


Figure 3.4 Block and principle electrical diagram of the system for temperature control and energy consumption measurement

The system also integrates an eight-channel temperature module (8CH DS18B20), which collects data from up to eight temperature sensors (Sensor 1 – Sensor 4 shown) and transmits them to the STM32 via the same RS485 bus. All components of the low-voltage part are powered by a stabilized 12V DC source, converted from 230V AC by power supply unit 1. The STM32 microcontroller collects, processes and transmits the data to a computer via a USB interface for visualization, configuration and archiving purposes.

In view of the presented subsystems and their functions, Figure 3.4 - A presents the overall configuration of the laboratory bench after its automation with all the hardware components considered. In this completed form, after the finalization, the bench is implemented as a fully functioning laboratory system, allowing remote control, real-time parameter monitoring and conducting experiments with high accuracy and reliability.



Figure 3.4 – A. Overall configuration of the laboratory stand after refinement and automation

SYSTEM COMPONENTS:

- 1. Outlet the end point of the air flow after heat treatment;
- 2. Outlet temperature heater includes a thermostat 1, a sensor and a heating element 1, which regulates and maintains the air temperature at the outlet;
- 3. Air valve allows manual adjustment of the opening to adjust the air volume;
- 4. Fan;
- 5. Intelligent electrical parameter meter;
- 6. Air inlet the point from which air enters the processing system;
- 7.1. Temperature sensor 1 intended for future convection measurements;
- 7.2. Temperature sensor 2 intended for future convection measurements;
- 7.3. Temperature sensor 3 air temperature after the heater;
- 7.4. Temperature sensor 4 air temperature before the heater;
- 8. Pitot tube with differential pressure measurement position;
- 9. Inlet heater;
- 10. Stepper motor (driver) for the Pitot tube TB6600;
- 11. Electric motor for driving the Pitot Tube
- 12. Positioning module for the Pitot Tube;
- 13. Thermal controller WS-T01-2;
- 13. Frequency servo drive TWS-02;
- 14. Differential pressure sensor QDF70B;
- 15. Electric energy meter (ENERGY METER);
- 17. Node-RED software for remote control and monitoring;
- 18. Lenovo ThinkCenter Server;
- 19. Automatic fuse;
- 20. Communication microcontroller STM 32;
- 21. Temperature converter AMDSG08.

3.3 Software description

The "Server" section presents the most important elements of building the data collection and processing system, with emphasis on the central server, remote power management, and the Node-RED application server.

Here, the possibility of centralized management is implemented, in which a Lenovo ThinkCentre computer acts as a main node, providing collection, storage and visualization of measurement data. It is indicated that it is configured with a local and external IP address and is connected to the internal network of Plovdiv University "Paisiy Hilendarski", thus achieving remote access and reliable management of the stand.

Particular attention is paid to the remote switching of the power supply, implemented using the Modbus over TCP/IP protocol and an eight-channel relay. Control commands in HEX format allow for safe switching on and off of the contactor and the server itself. This is illustrated in Figure 3.5.

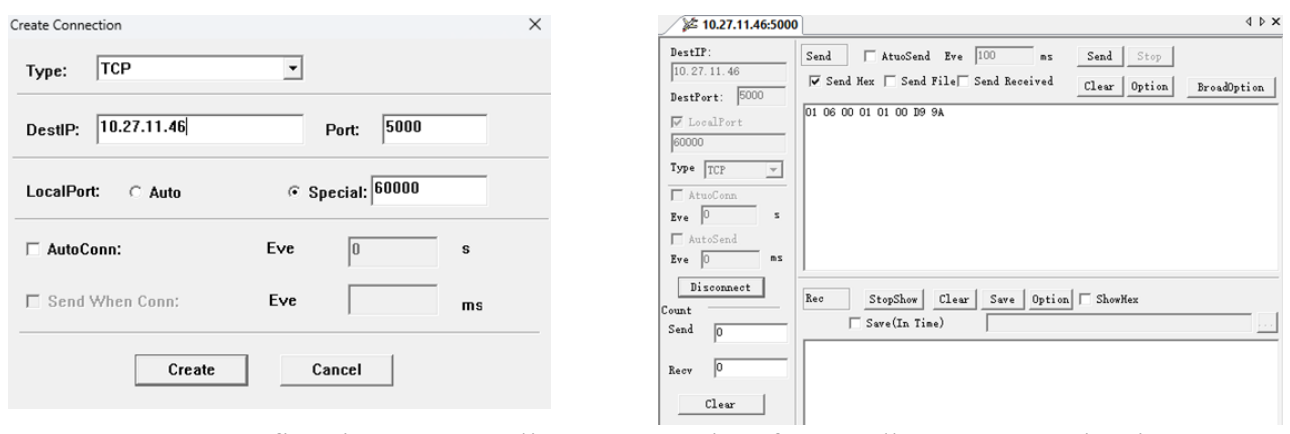


Figure 3.5 Configuring a TCP client connection for Modbus communication and sending a Modbus command in HEX format to a device via TCP interface

The architecture of the software part is divided into three main sections (Figure 3.6): thread 1 for the physical sensors, thread 2 for communication, and Node-RED for visualization and control.

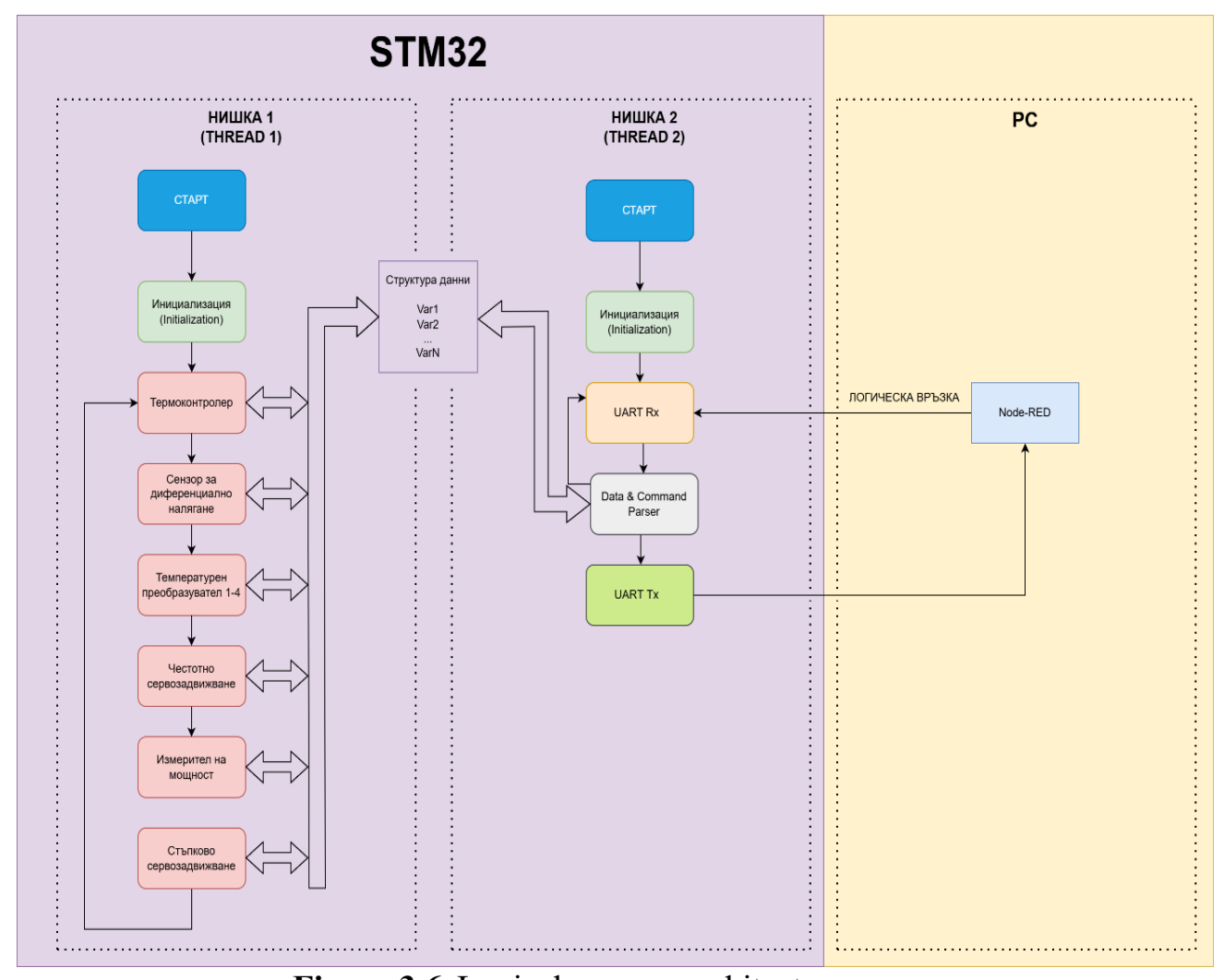


Figure 3.6 Logical process architecture

The first thread is responsible for managing all the physical sensors and actuators that are connected to the system. This thread includes the following key blocks:

- **Thermal controller** serves to control a heating element by regulating the temperature based on measurements from temperature transducers;
- **Differential pressure sensor** measures the pressure difference between two points in the system;
- **Temperature transducers 1–4** measure the temperature of different sections or elements of the system;
- Frequency servo drive (inverter)— controls the rotation speed of a motor or fan based on preset values;
- **Power meter** records the current electrical consumption and feeds it to the logic for analysis and average value;
- Stepper servo drive (positioning mechanism)— adjusts the physical position of the Pitot tube based on input commands.

The data from all these hardware components is structured into an organized array of variables (Var1, Var2, ..., VarN), which is used to communicate with the second thread via an internal program connection.

The second thread takes on the task of communicating between the hardware part and the external interface (the personal computer where Node-RED is located). It includes the following main blocks:

- UART Rx (Universal Asynchronous Receiver) receives data from Node-RED (PC) via serial interface. Receives commands and parameters for executing processes.
- UART Tx (transmitter) sends information back to the external Node-RED server. This information includes command execution confirmations, current sensor values, and diagnostic messages that are used for operator visualization and monitoring.
- Data & Command Parser is responsible for decoding and processing the input data. In addition to measurement values, this block also accepts commands sent by the operator through the user interface in Node-RED (e.g. setting a position, turning a module on/off, etc.). The data is interpreted and structured, and the results are directed to the appropriate hardware modules or prepared for reverse visualization.

The third part of the architecture is the Node-RED application server, which is installed on a personal computer. It makes a logical connection with thread 2 and performs several key functions. First of all, Node-RED is responsible for data visualization - all values received from sensors are presented in real time through graphs, indicators, text elements and other visual tools that facilitate monitoring of the system status.

An important part of the section are the logic flows implemented in Node-RED, which show how data is processed and how the individual subsystems are managed. They are presented sequentially in Figures 3.7, 3.8, 3.9 and 3.10.

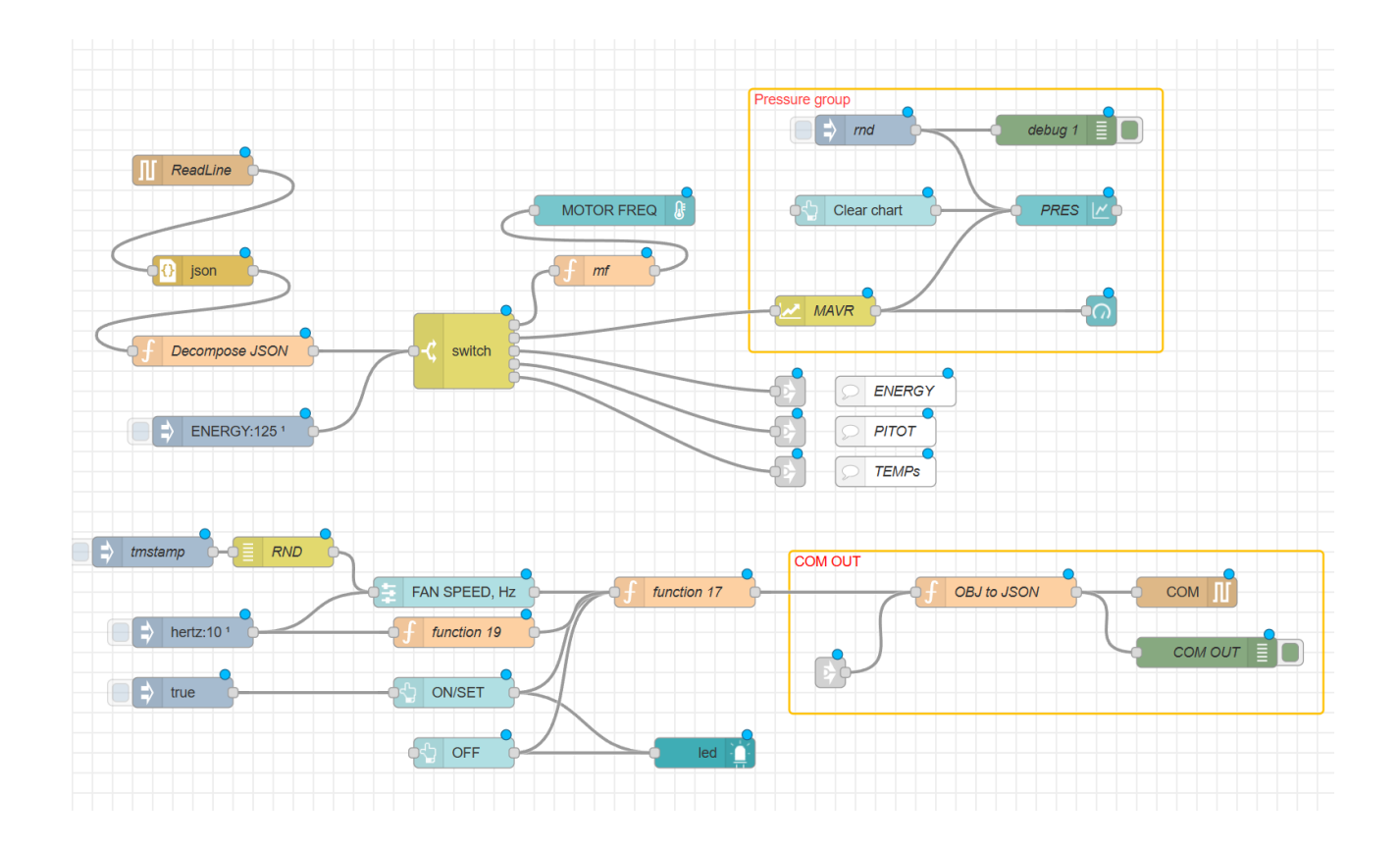


Figure 3.7 Basic data processing, visualization and communication in Note-RED

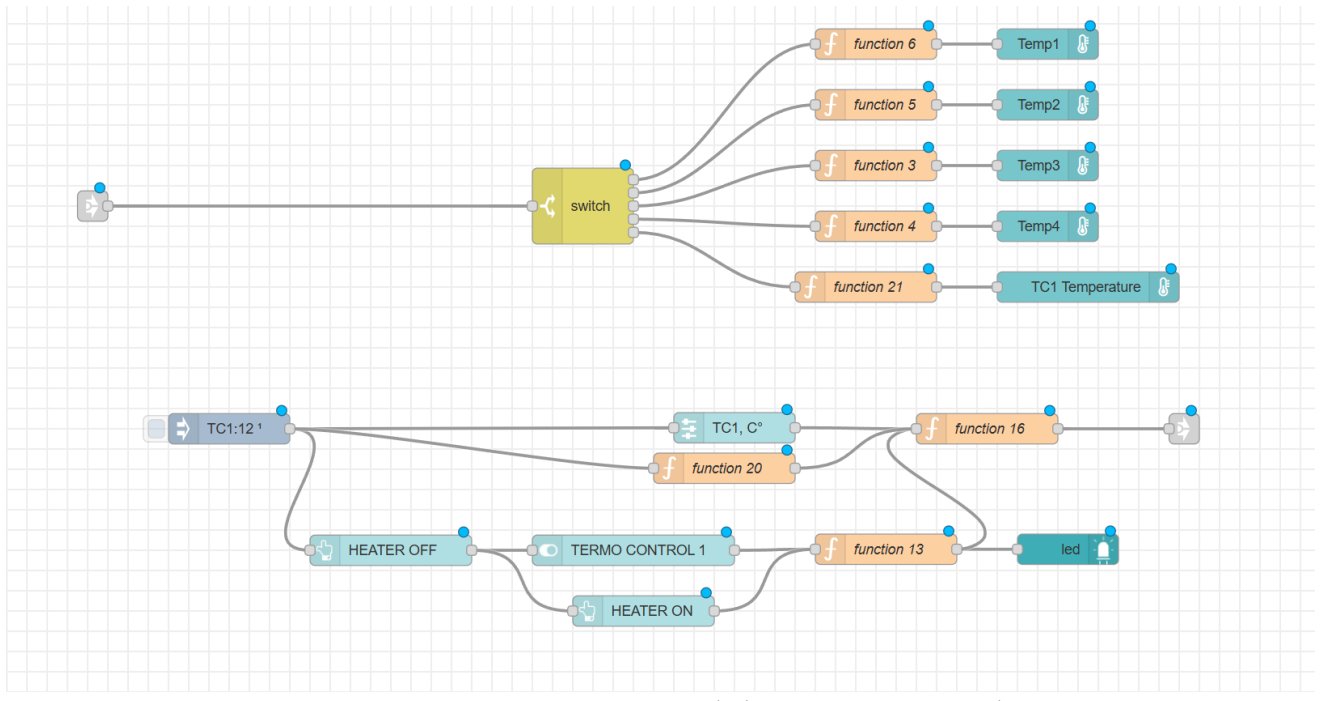


Figure 3.8 Temperature and thermostat control

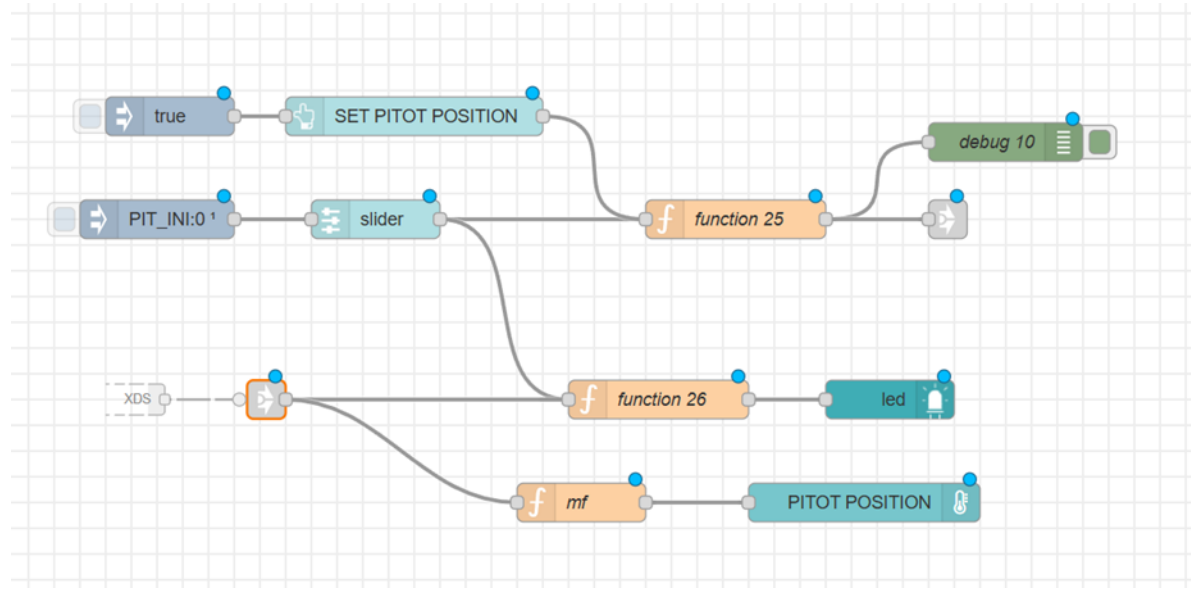


Figure 3.9 Pitot tube position control

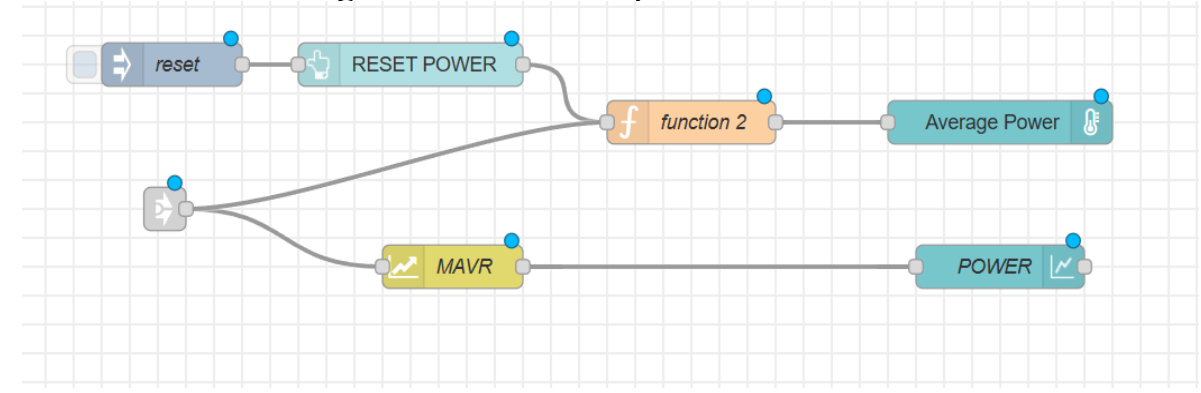


Figure 3.10 Measurement and control of electrical power

3.4 CONCLUSIONS OF CHAPTER 3

Chapter 3 discusses the development and implementation process of the automated laboratory bench with remote access capability, focusing on the hardware structure, communication architecture, and software integration. A modular and scalable solution has been implemented, allowing for complex measurement and control tasks through a centralized microcontroller system.

The selected microcontroller STM32F103ZE is justified as an optimal solution that provides a balance between computing power, reliability and communication interfaces. Robust communication processes are implemented via Modbus RTU and TCP/IP, which ensures compatibility with SCADA and IoT platforms. Remote power control via an eight-channel relay is introduced, which ensures safety and efficiency, and the integrated frequency servo drive, temperature converters and sensors allow for precise control and reliable measurements.

An energy monitoring system has also been implemented, providing accurate information on consumption and energy efficiency. The implementation of Node-RED provides an intuitive visual environment for monitoring and management, allowing two-way communication, real-time visualization and active interaction with the operator.

The result is a sustainable and flexible platform that has proven to be useful in both educational and scientific environments, as well as in industrial applications where reliability, automation, and remote access are required.

CHAPTER 4. EXPERIMENTAL RESEARCH

This chapter of the dissertation presents the results of the experimental studies conducted related to the validation of the developed automated laboratory system and its applicability. The purpose of these studies is to confirm the functionalities of the methodologies described in CHAPTER 2, to test the hardware designed in CHAPTER 3 and to analyze the results in the context of the used measuring equipment and automated means for recording and controlling the processes.

4.1.1 Experimental determination of the air flow velocity profile in a rectangular pipe. Determination of the air flow rate in the measured cross section.

Before the actual measurements begin, it is necessary to perform preliminary preparation of the system in remote mode, both by the instructor and by the participants in the experiment. The procedure includes the following main steps:

- 1. Joining the video conference connection provided by the instructor;
- 2. Waiting for the teacher to remotely turn on the server, control panel and stand;
- 3. Launching the SmartPSS Lite application by the user and performing a visual check of the stand's operability, by:
 - ♣ Setting different Pitot tube positions through the interface;
 - ♣ Tracking the execution of commands and their correspondence with real movements;
 - ♣ Monitoring the update of the pressure and position readings in the Node-RED system.

This preliminary phase is key to ensuring the reliability of the remote connection and the full functionality of the automated system before starting the experimental process.

> Air density measurement

Measurements must be standardized to the SI system. Density ρ is determined by the equation of state of the ideal gas (2.7):

$$\rho = \frac{P_{\text{atm}}}{R.T}$$

where:

- P_{atm} is the atmospheric pressure (Pa);
- R=287.05 J/(kg.K) is the gas constant for air;
- Tis the temperature in Kelvin (T=T_{измерена} +273.15).

For determining the value of air density ρ according to formula 2.7 is required from sinoptik.bg (LINK: https://www.sinoptik.bg/plovdiv-bulgaria-100728193) to take the value of P_{atm} for the city of Plovdiv at the current moment of measurement ($P_{\text{atm}} = 1020.98 \text{ hPa}$). It changes depending on the altitude, temperature and humidity of the air. It is measured in pascals (Pa), but in practice in metrology it is most often measured in hectopascals (1 hPa = 100 Pa). For $T_{\text{измерена}}$ we read the value of Temp4 (ambient temperature) from the TEMPERATURES section of the visual interface of the Node-RED

software application. In our case $T_{\mu_{3Meperal}} = 26.1^{\circ}$ C. We convert the temperature from Celsius to Kelvin and substitute into the formula for air density:

$$T=T_{\text{измерена}}+273.15=26.1+273.15=299.25 \text{ K}$$

The value of air density ρ we find by formula 2.7:

$$\rho = \frac{P_{\text{atm}}}{R.T} = \frac{1020,98.100}{287,05.299,25} = \frac{102098}{85899.71} = 1.19 \, kg/m^3$$

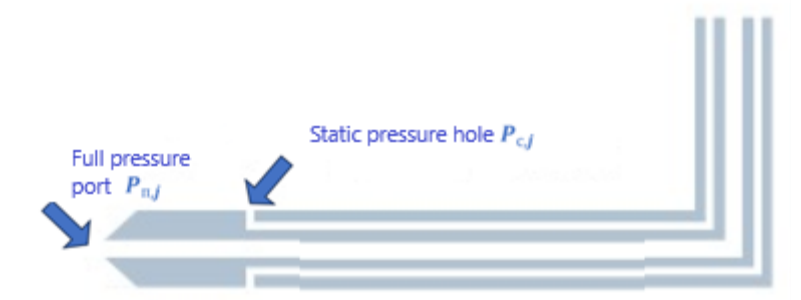
 \triangleright Calculation of air flow velocity for each measurement point v_i

The air velocity for each measurement point is found by formula (2.8):

$$v_j = \sqrt{\frac{2.(P_{\pi,j} - P_{c,j})}{\rho}},$$

where:

- v_i is the air flow velocity (m/s) at point j of the measured cross section that we want to calculate;
- P_{π,j} is the total pressure (Pa) at point j, measured with the Pitot tube
 P_{c,j} is the static pressure (Pa) at point j, also measured with the Pitot tube;
- $\Delta P_{A,j}$ is the dynamic pressure (Pa) at point j, which is the difference between the total pressure $P_{\pi,i}$ and the static pressure $P_{c,i}$;
- ρ is the air density (kg/m³), which is considered constant in the measured cross-section. It is defined in the previous paragraph.



Schematic layout of the Pitot tube holes Figure 4.1

In the present analysis, the air flow velocity is measured at 5 points located at different distances from the wall of the duct (Figure 2.6 of CHAPTER 2), and at different frequencies of the asynchronous electric motor. Increasing the supply frequency of the electric motor leads to a proportional increase in the rotation frequency of the fan integrated in the system, which in turn causes an increase in the volumetric flow rate of the suction air. This change has a direct impact on the differential pressure values and, consequently, on the air flow velocities measured at the selected points of the cross section.

For each frequency, measurements are made using a Pitot tube, and the velocity value is calculated using formula (2.8) using the air density value, also obtained using formula (2.7).

The measurements are carried out at four different frequencies: 20 Hz, 40 Hz, 60 Hz and 80 Hz. At the same time, the developed software application, through the CONTROLS section, SET DEPTH subsection, controls and positions the Pitot tube at each of the five defined measurement points, visually presented in Figure 2.6 of CHAPTER 2.

The differential pressure value is read from the PRESSURE control panel of the application ΔP_{π} after the transient process is completed at given frequencies of the induction motor. The points are located along the height of the square hole, at distances of 8 mm, 25 mm, 42 mm, 58 mm and 75 mm, with 75 mm corresponding to the center of the section. The measurements will be made at four separate frequencies of the induction motor - 20 Hz, 40 Hz, 60 Hz and 80 Hz, and the speeds will be calculated for each of the five measurement points at the different frequencies.

Table 4.1	velocity and volume flow distribution at 20 Hz frequency

Distance from the wall	ΔP _д Yes	v _i m/s				
8mm	3	$v_1 = \sqrt{\frac{2.(P_{\pi,1} - P_{c,1})}{\rho}} = \sqrt{\frac{2.(\Delta P_{\pi,1})}{\rho}} = \sqrt{\frac{2.(3)}{1.19}} = \sqrt{\frac{6}{1.19}} = \sqrt{5.0420} = 2.25$ m/s				
25 mm	4	$v_2 = \sqrt{\frac{2.(P_{\pi,2} - P_{c,2})}{\rho}} = \sqrt{\frac{2.(\Delta P_{\pi,2})}{\rho}} = \sqrt{\frac{2.(\Delta P_{\pi,2})}{1.19}} = \sqrt{\frac{8}{1.19}} = \sqrt{6.722} = 2.59$ m/s				
42 mm	4	$v_3 = \sqrt{\frac{2.(P_{\pi,3} - P_{c,3})}{\rho}} = \sqrt{\frac{2.(\Delta P_{\pi,3})}{\rho}} \sqrt{\frac{2.(4)}{1.19}} = \sqrt{\frac{8}{1.19}} = \sqrt{6.722} = 2.59$ m/s				
58 mm	4	$v_4 = \sqrt{\frac{2.(P_{\pi,4} - P_{c,4})}{\rho}} = \sqrt{\frac{2.(\Delta P_{\pi,4})}{\rho}} \sqrt{\frac{2.(4)}{1.19}} = \sqrt{\frac{8}{1.19}} = \sqrt{6.722} = 2.59$ m/s				
75mm	4	$v_5 = \sqrt{\frac{2.(P_{\pi,5} - P_{c,5})}{\rho}} = \sqrt{\frac{2.(\Delta P_{\pi,5})}{\rho}} = \sqrt{\frac{2.(\Delta)}{1.19}} = \sqrt{\frac{8}{1.19}} = \sqrt{6.722} = 2.59$ m/s				

Table 4.2 Speed and volume flow distribution at 40 Hz frequency

Distance from the wall	ΔP _д Yes	v_{j} m/s
8mm	13	$v_1 = \sqrt{\frac{2.(P_{\pi,1} - P_{c,1})}{\rho}} = \sqrt{\frac{2.(\Delta P_{\pi,1})}{\rho}} = \sqrt{\frac{2.(13)}{1.19}} = \sqrt{\frac{26}{1.19}} = \sqrt{21.84} = 4.67$ m/s
25 mm	16	$v_2 = \sqrt{\frac{2.(P_{\pi,2} - P_{c,2})}{\rho}} = \sqrt{\frac{2.(\Delta P_{\pi,2})}{\rho}} = \sqrt{\frac{2.(16)}{1.19}} = \sqrt{\frac{32}{1.19}} \sqrt{26.89} = 5.19$ m/s
42 mm	17	$v_3 = \sqrt{\frac{2.(P_{\text{n,3}} - P_{\text{c,3}})}{\rho}} = \sqrt{\frac{2.(\Delta P_{\text{p,3}})}{\rho}} = \sqrt{\frac{2.(17)}{1.19}} = \sqrt{\frac{34}{1.19}} = \sqrt{\frac{28.57}{1.19}} = 5.35$

Distance from the wall	ΔP _д Yes	v _i m/s
58 mm	18	$v_4 = \sqrt{\frac{2.(P_{\pi,4} - P_{c,4})}{\rho}} = \sqrt{\frac{2.(\Delta P_{\pi,4})}{\rho}} = \sqrt{\frac{2.(18)}{1.19}} = \sqrt{\frac{36}{1.19}} = \sqrt{30.25} = 5.5$ m/s
75mm	18	$v_5 = \sqrt{\frac{2.(P_{\text{n,5}} - P_{\text{c,5}})}{\rho}} = \sqrt{\frac{2.(\Delta P_{\text{n,5}})}{\rho}} = \sqrt{\frac{2.(18)}{1.19}} = \sqrt{\frac{36}{1.19}} = \sqrt{30.25} = 5.5$ m/s

 Table 4.3
 Speed and volume flow distribution at 60 Hz frequency

DEPTH	$\Delta P_{_{ m I\! I}}$	v_{i}
8mm	22	$v_1 = \sqrt{\frac{2.(P_{\text{n,1}} - P_{\text{c,1}})}{\rho}} = \sqrt{\frac{2.(\Delta P_{\text{p,1}})}{\rho}} = \sqrt{\frac{2.(22)}{1.19}} = \sqrt{\frac{44}{1.19}} = \sqrt{36.97} = 6.08$ m/s
25 mm	36	$v_2 = \sqrt{\frac{2.(P_{\pi,2} - P_{c,2})}{\rho}} = \sqrt{\frac{2.(\Delta P_{\pi,2})}{\rho}} = \sqrt{\frac{2.(36)}{1.19}} = \sqrt{\frac{72}{1.19}} \sqrt{60.50} = 7.78$ m/s
42 mm	39	$v_3 = \sqrt{\frac{2.(P_{\pi,3} - P_{c,3})}{\rho}} = \sqrt{\frac{2.(\Delta P_{\pi,3})}{\rho}} = \sqrt{\frac{2.(39)}{1.19}} = \sqrt{\frac{78}{1.19}} = \sqrt{\frac{65.54}{65.54}} = 8.10$
58 mm	40	$v_4 = \sqrt{\frac{2.(P_{\text{II},4} - P_{\text{C},4})}{\rho}} = \sqrt{\frac{2.(\Delta P_{\text{II},4})}{\rho}} = \sqrt{\frac{2.(40)}{1.19}} = \sqrt{\frac{80}{1.19}} = \sqrt{67.22} = 8.20$ m/s
75mm	40	$v_5 = \sqrt{\frac{2.(P_{\pi,5} - P_{c,5})}{\rho}} = \sqrt{\frac{2.(\Delta P_{\pi,5})}{\rho}} = \sqrt{\frac{2.(40)}{1.19}} = \sqrt{\frac{80}{1.19}} = \sqrt{67.22} = 8.2$ m/s

 Table 4.4
 Velocity and volume flow distribution at 80 Hz frequency

	$\Delta P_{\rm g}$	v_{i}
H		
8mm	45	$v_1 = \sqrt{\frac{2.(P_{\pi,1} - P_{c,1})}{\rho}} = \sqrt{\frac{2.(\Delta P_{\mu,1})}{\rho}} = \sqrt{\frac{2.(45)}{1.19}} = \sqrt{\frac{90}{1.19}} = \sqrt{75.63} = 8.70 \text{ m/s}$
25 mm	55	$v_2 = \sqrt{\frac{2.(P_{\pi,2} - P_{c,2})}{\rho}} = \sqrt{\frac{2.(\Delta P_{\pi,2})}{\rho}} = \sqrt{\frac{2.(55)}{1.19}} = \sqrt{\frac{110}{1.19}} \sqrt{92.43} = 9.61 \text{ m/s}$
42 mm	66	$v_3 = \sqrt{\frac{2.(P_{\pi,3} - P_{c,3})}{\rho}} = \sqrt{\frac{2.(\Delta P_{\pi,3})}{\rho}} = \sqrt{\frac{2.(66)}{1.19}} = \sqrt{\frac{132}{1.19}} = \sqrt{110.92} = 10.53$ m/s
58 mm	67	$v_4 = \sqrt{\frac{2.(P_{\pi,4} - P_{c,4})}{\rho}} = \sqrt{\frac{2.(\Delta P_{\pi,4})}{\rho}} = \sqrt{\frac{2.(67)}{1.19}} = \sqrt{\frac{134}{1.19}} = \sqrt{112.60} = 10.61$ m/s

DEPT H	$\Delta P_{_{ m II}}$	v_{i}
75mm	67	$v_5 = \sqrt{\frac{2.(P_{\text{n,5}} - P_{\text{c,5}})}{\rho}} = \sqrt{\frac{2.(\Delta P_{\text{p,5}})}{\rho}} = \sqrt{\frac{2.(67)}{1.19}} = \sqrt{\frac{134}{1.19}} = \sqrt{112.60} = 10.61$ m/s

4.1.1 Determining the air flow rate in the measured cross section $w(m^3/s)$

The air flow in different zones is calculated based on the air velocity and the area of the cross-section through which it passes. The diagram presented in Figure 2.6 of CHAPTER 2 shows the location of the square regions with real areas and their corresponding cross-sections. Each measured cross-section has fixed dimensions that determine its real values. The formulas for calculating the areas and flows are as follows (formulas 2.9 to 2.13):

$$A_1 = 150^2 (mm) - 117^2 (mm) = 22500 - 13685 = 8811mm2.10-6=0.00881 \ m2;$$

 $A_2 = 117^2 (mm) - 83^2 (mm) = 13689 - 6889 = 6800 \ mm2.10-6 = 0.0068 \ m2;$
 $A_3 = 83^2 (mm) - 50^2 (mm) = 6889 - 2500 = 4389 \ mm2.10-6 = 0.004389 \ m2;$
 $A_4 = 50^2 (mm) - 17^2 (mm) = 2500 - 289 = 2211 \ mm2.10-6 = 0.002211 \ m2;$
 $A_5 = 17 \ (mm) \cdot 17 \ (mm) = 289 \ mm2 \cdot 10-6=0.000289 \ m2.$

To calculate the airflow in each zone $w(m^3/s) = A(m^2) \cdot v(m/s)$ by formulas (2.14 – 2.18) from CHAPTER 2 we substitute, the calculation is performed separately at the different frequencies of the asynchronous motor and the graphs of the dependencies are plotted.

ightharpoonup Calculation of air flow in the measured cross section $w(m^3/s)$ at a motor frequency of 20 Hz

$$w_1 = v_1 \cdot A_1 = 2.25 \cdot 0.008811 = 0.01978m^3/s$$

 $w_2 = v_2 \cdot A_2 = 2.59 \cdot 0.0068 = 0.01763m^3/s$
 $w_3 = v_3 \cdot A_3 = 2.59 \cdot 0.004389 = 0.01138m^3/s$
 $w_4 = v_4 \cdot A_4 = 2.59 \cdot 0.002211 = 0.00573m^3/s$
 $w_5 = v_5 \cdot A_5 = 2.59 \cdot 0.000289 = 0.00075m^3/s$

The total air flow for all sections at 20 Hz frequency of the electric motor is found by formula (2.19) as follows:

$$\mathbf{w}_{A} = w_{1} + w_{2} + \dots w_{i} = \sum_{i=1}^{5} w_{i}$$

$$\mathbf{w}_{A} = w_{1} + w_{2} + w_{3} + w_{4} + w_{5}$$

$$w_{A} = 0.01978 + 0.01763 + 0.01138 + 0.00573 + 0.00075$$

$$\mathbf{w}_{A} = \mathbf{0.05528} \ \mathbf{m}^{3} / \mathbf{s}$$

The calculations of the air flow in the measured cross-section were made in a similar way $w(m^3/s)$ for electric motor frequencies of 40 Hz, 60 Hz and 80 Hz.

4.1.2 Presentation of measurement results

Based on the experimental measurements, the data obtained characterize the distribution of the velocity and volumetric flow rate of the air flow at different operating frequencies of the system. In order to present the obtained experimental results in a clearer and more structured way, the data are organized in four separate tables – 4.5 ... 4.8, corresponding to each of the studied rotation frequencies – 20 Hz, 40 Hz, 60 Hz and 80 Hz. Each table includes the measured values of the differential pressure, the calculated velocity of the air flow and the corresponding volumetric flow rate for five different measurement depths.

Table 4.5 Velocity and volume flow distribution at a servo frequency of 20 Hz and air density $\rho = 1.19 \, kg / m^3$

DEPTH	A_j	(m^2)	$\Delta P_{A,j}(Pa)$	v_{i}	(m/s)	w_i	(m^3/s)
8mm	A 1	0.008811	3	v_1	2.25	w_1	0.01978
25 mm	A2	0.0068	4	v_2	2.59	W_2	0.01763
42 mm	A3	0.004389	4	v_3	2.59	W_3	0.01138
58 mm	A4	0.002211	4	v_4	2.59	W_4	0.00573
75mm	A5	0.000289	4	v_5	2.59	W_5	0.00075
		Tot	0.05528				

Table 4.6 Velocity and volume flow distribution at a servo drive frequency of 40 Hz and air density $\rho = 1.19 \, kg / m^3$

DEPTH	A_{j}	(m^2)	$\Delta P_{A,j}(Pa)$	v_{j}	(m/s)	w_i	(m^3/s)
8mm	A 1	0.008811	13	v_1	4.67	w_1	0.04115
25 mm	A2	0.0068	16	v_2	5.19	w_2	0.03529
42 mm	A3	0.004389	17	v_3	5.35	W_3	0.02346
58 mm	A4	0.002211	18	v_4	5.50	W_4	0.01216
75mm	A5	0.000289	18	v_5	5.50	W_5	0.00159
		Tot	0.11365				

Table 4.7 Velocity and volume flow distribution at 60 Hz servo frequency and air density $\rho = 1.19 \, kg / m^3$

DEPTH	A_{j}	(m^2)	$\Delta P_{A,j}(Pa)$	v_{j}	(m/s)	w_i	(m^3/s)	
8mm	A 1	0.008811	22	v_1	6.08	w_1	0.05358	
25 mm	A2	0.0068	36	v_2	7.78	w_2	0.05289	
42 mm	A3	0.004389	39	v_3	8.10	W_3	0.03553	
58 mm	A4	0.002211	40	v_4	8.20	W_4	0.01813	
75mm	A5	0.000289	40	v_5	8.20	W_5	0.00237	
		Total air flow for the sections - W_A 0.16250						

Table 4.8 Velocity and volume flow distribution at servo frequency 80 Hz and air density $\rho = 1.19 \, kg / m^3$

DEPTH	A_{j}	(m^2)	$\Delta P_{A,j}(Pa)$	v_{i}	(m/s)	w_i	(m^3/s)
8mm	A 1	0.008811	45	v_1	8.70	w_1	0.07663
25 mm	A2	0.0068	55	v_2	9.61	W_2	0.06538
42 mm	A3	0.004389	66	v_3	10.53	W_3	0.04623
58 mm	A4	0.002211	67	v_4	10.61	W_4	0.02346
75mm	A5	0.000289	67	v_5	10.61	W_5	0.00307
		Total air flow for the sections - W_A 0					0.21476

After presenting the experimental results in tabular form, based on the initial data and using Microsoft Excel, we visualize graphs that reflect the dependencies between the volumetric flow rate and the air flow velocity at different operating frequencies. These dependencies are shown in the following figures 4.2 ... 4.5 and illustrate the characteristic flow profiles for each of the frequencies considered.

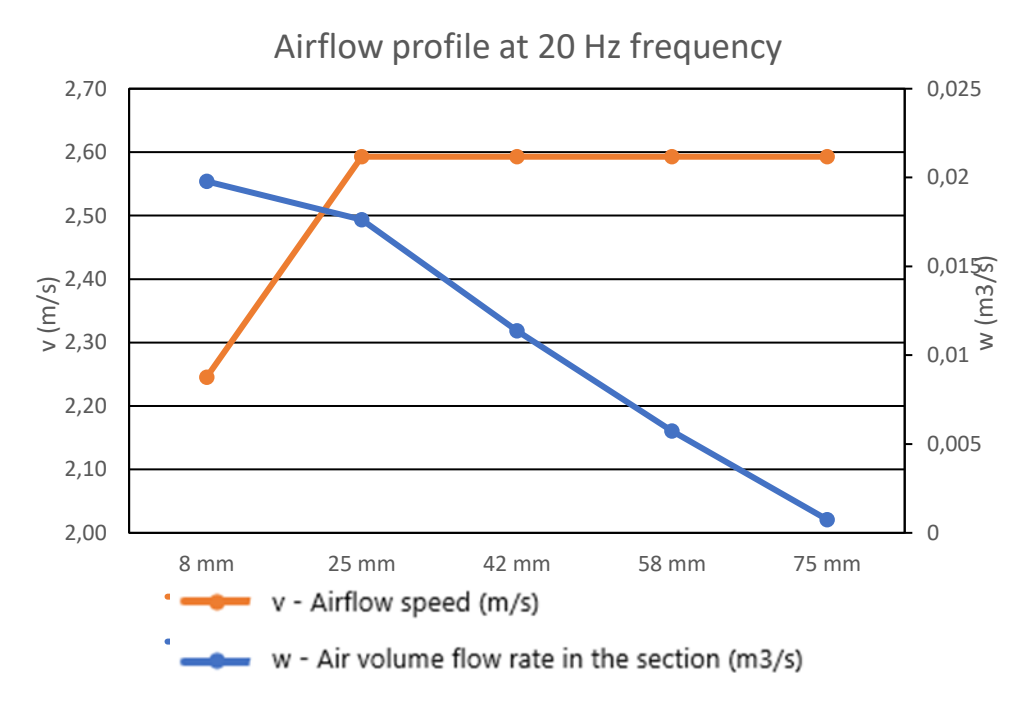


Figure 4.2 Airflow profile at frequency servo drive 20 Hz

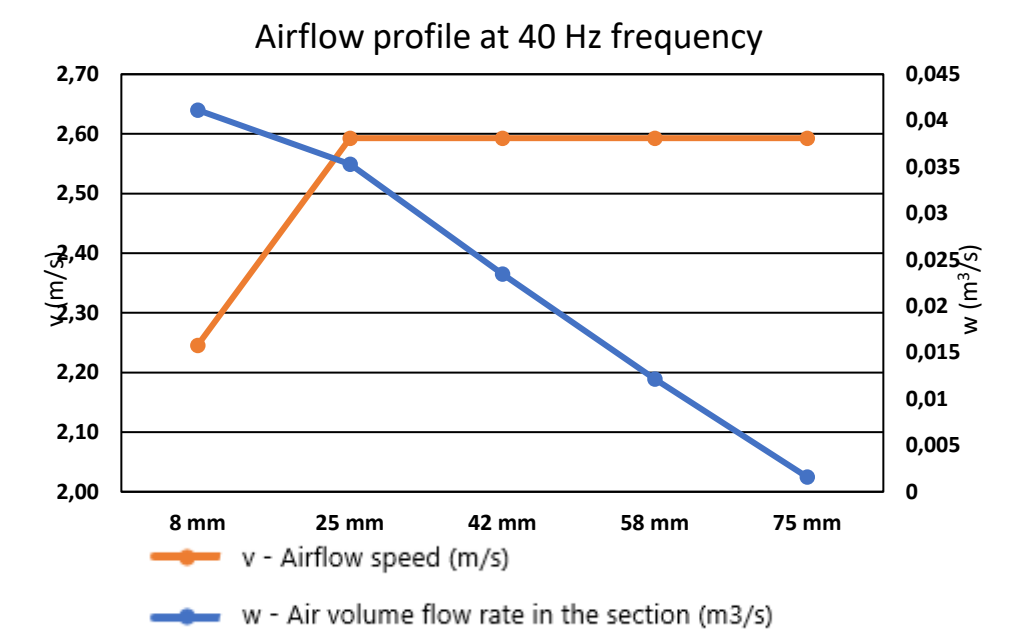


Figure 4.3 Airflow profile at frequency servo drive 40 Hz

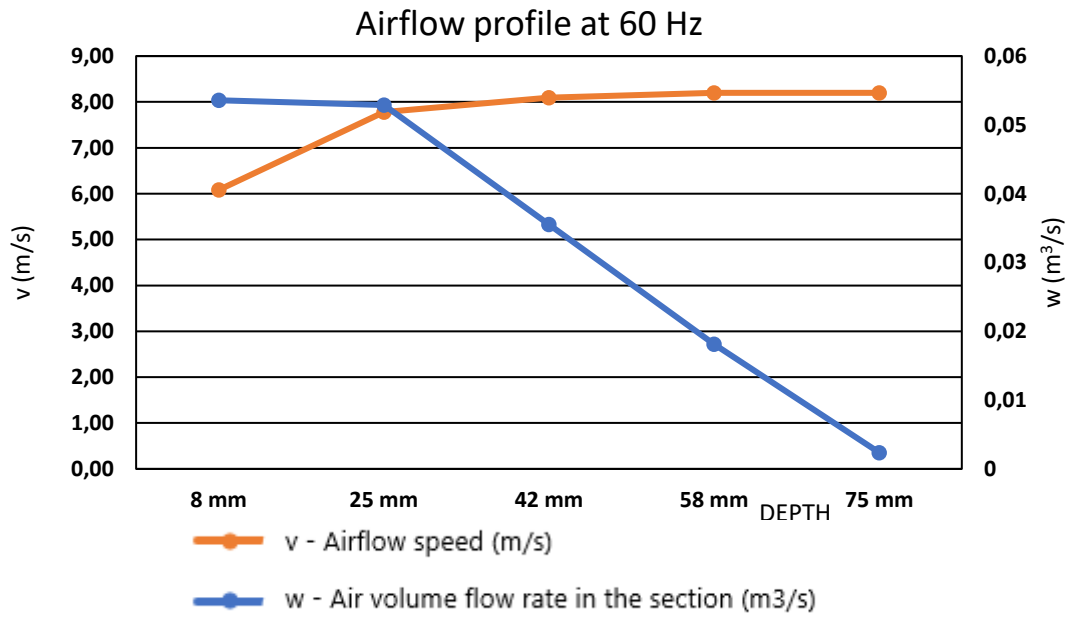


Figure 4.1 Airflow profile at frequency servo drive 60 Hz

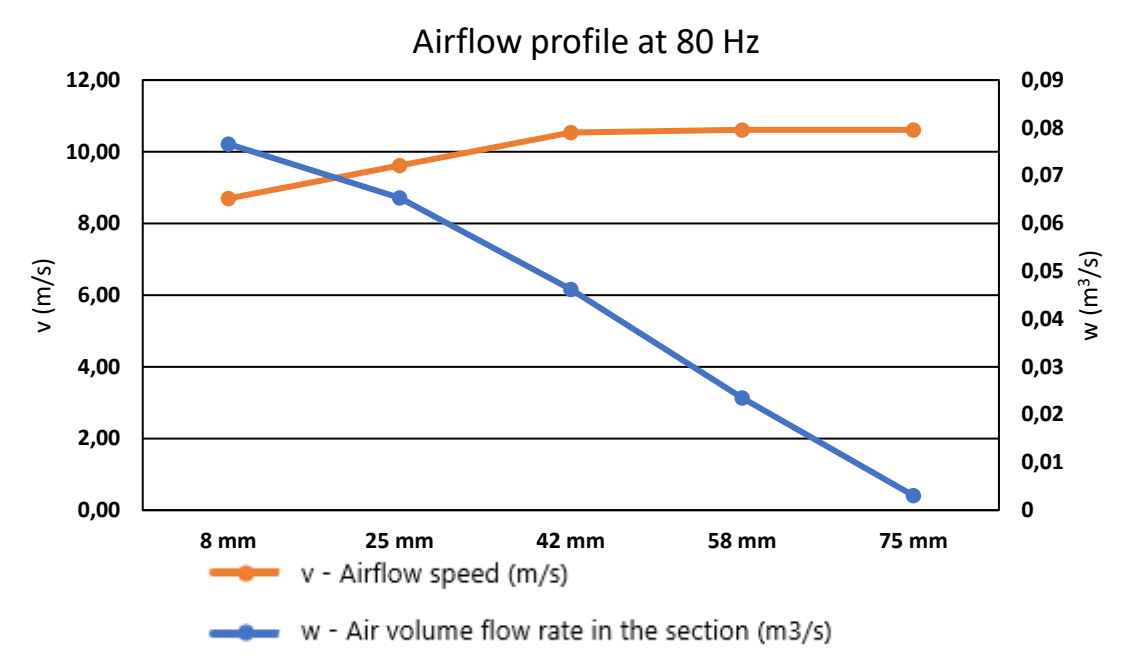


Figure 4.2 Airflow profile at frequency servo drive 80 Hz

After presenting the airflow profiles at each frequency, we also visualize a summary graph that presents the relationship between volumetric flow rate and airflow velocity at the measurement point. v_5 This point is located in the central zone of the flow, at a depth of 75 mm, and is indicative of the behavior of the flow in its most intense part.

Figure 4.6 presents a linear approximation of the relationship between volumetric flow rate $\mathbf{w_A}$ and the speed at a point $\mathbf{v_5}$ The data were obtained at the four studied frequencies -20, 40, 60 and 80 Hz. The obtained regression function is of the form:

$$w_A = 0.0197 v_5 + 0.0041$$

with a coefficient of determination R2 = 0.999, which indicates an extremely good linear relationship between speed and volumetric flow rate at this point.

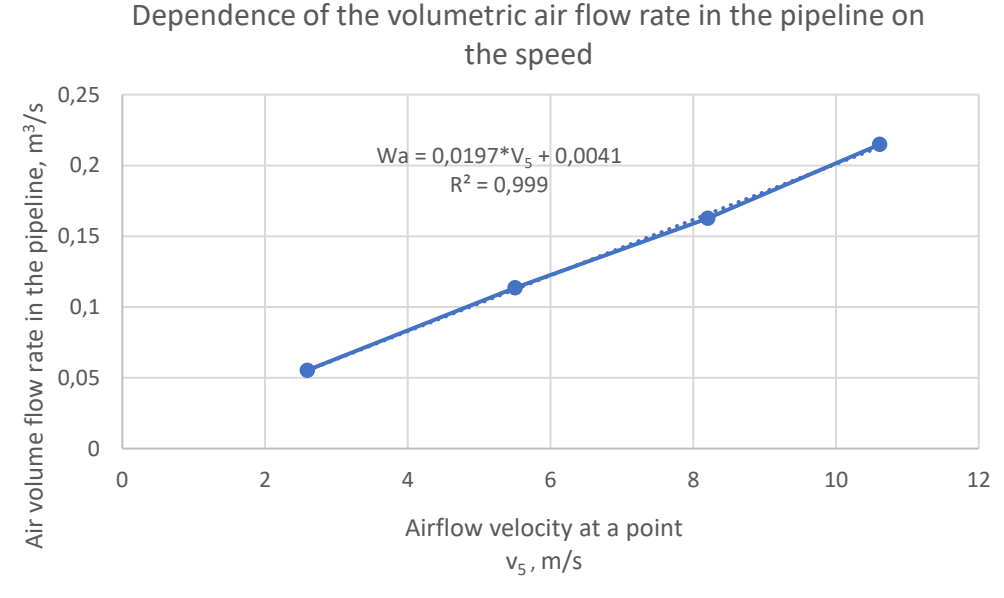


Figure 4.3 Approximation of the dependence of \mathbf{w} from \mathbf{v} \mathbf{D}

The graph demonstrates a clearly expressed linear trend: with increasing speed at a point v_5 , the volumetric flow rate increases proportionally. This behavior is fully

consistent with the theoretical expectations based on the continuity equation and confirms the reliability of the measurements.

4.2 Experimental determination of the mass specific heat capacity of air at constant pressure

As in the procedure described in Methodology 2.3, as well as in the present experiment, before the start of the actual measurements, it is necessary to carry out targeted preliminary preparation of the system in remote mode, the block diagram of which is presented in Figure 2.5 in CHAPTER 2. The purpose of this preparation is to guarantee the functional integrity of the laboratory stand, as well as the reliable visualization and reporting of the main measurement parameters through a developed software interface.

4.2.1 Analytical calculations at 20 Hz frequency

After completion of the adjustment and stabilization phase of the regime, as described in the experimental methodology, calculations are performed to determine the thermal and energy parameters of the air at the supply frequency of the asynchronous electric motor of 20 Hz, 40 Hz, 60 Hz and 80 Hz. The measurements were carried out on 11.08.2025 in the "Eco-Energy Technologies" laboratory at the "Paisiy Hilendarski" Plovdiv University.

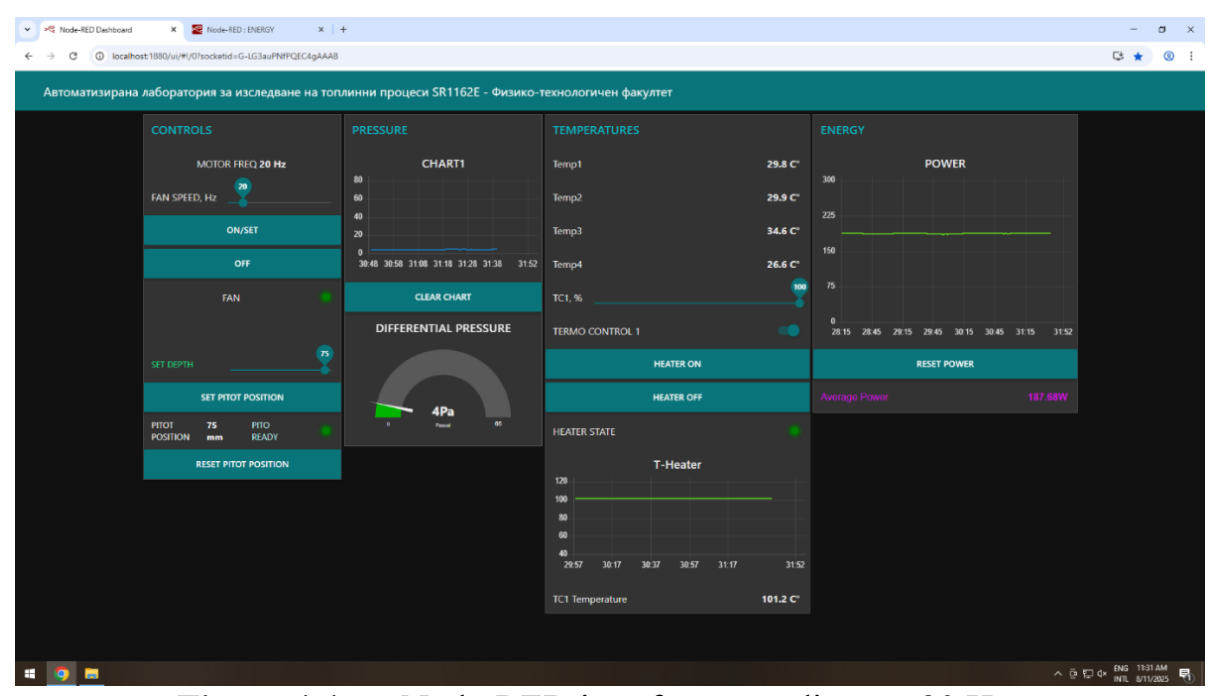


Figure 4.4 Node-RED interface – readings at 20 Hz

Based on the values from figure 4.7 (Temp3 = 34.6 °C, Temp4 = 26.6 °C, Average Power $\dot{Q} = 187.68 \ W$, $\Delta P_{\rm A} = 4 \ Pa$) and air density $\rho = 1.18 \ {\rm kg/m^3}$ (calculated in methodology 2.2 based on the current value of the ambient temperature), as well as the actual diameter of the air duct d = 0.15 m (visualized in Figure 2.7 of CHAPTER 2) the following calculations are performed:

According to methodology 2.2, the value of the air density ρ is found by the formula:

$$\rho = \frac{P_{\text{atm}}}{R \ T}$$

where:

- P_{atm} is the current atmospheric pressure (Pa) for the day in the city of Plovdiv;
- R=287.05 J/(kg/K) is the gas constant for air;
- Tis the temperature in Kelvin (T = T_4 +273.15 = 26.6 + 273.15 = 299.75 K).

$$\rho = \frac{P_{\text{aTM}}}{R.T} = \frac{1018,73.100}{287,05.299,75} = \frac{101873}{85043.23} = 1.19 \, kg/m^3$$
The first step is to calculate the temperature difference in Kelvin relative to the Si

The first step is to calculate the temperature difference in Kelvin relative to the Si system before and after the heater between temperature sensor Temp3 (located after the heater T3=34.6 °C + 273.15=307.75 K) and temperature sensor Temp4 (located before the heater T4=26.6 °C + 273.15=299.75 K):

$$\Delta T = T_2 - T_4 = 307.75 - 299.75 = 8 K$$

Then, the air velocity is calculated according to Bernoulli's equation at a certain point in the cross section (in our case, the point is in the central position of the air duct with a distance of 75 mm from the wall), as:

$$v_5 = \sqrt{\frac{2.(P_{\pi,5} - P_{c,5})}{\rho}} = \sqrt{\frac{2.(\Delta P_{\pi,5})}{\rho}} = \sqrt{\frac{2.(4)}{1.19}} = \sqrt{\frac{8}{1.19}} = \sqrt{6.722} = 2.59 \text{ m/s}$$

$$\dot{m} = 0.0078 \text{ v} + 0.0016,$$

obtained after calibrating the bench and performing a linear approximation of the experimental data at $R^2 = 0.999$.

$$\dot{m}$$
= 0.0078.v5 + 0.0016 = 0.0078 . 2.59 + 0.0016 = 0.0218 kg/s

Next determining the heat input to 1 kg of air (here *Q* is equal to the average electrical power of the heater, read in the lower right corner of the "POWER" indicator marked as Average Power) ():

$$q = \frac{\dot{Q}}{\dot{m}} = \frac{187.68}{0.0218} = 8609 \,\text{J/kg}$$

Based on this, the average mass specific heat capacity is determined \bar{c} , using formula (2.22):

$$\bar{c} = \frac{q}{T_3 - T_4} = \frac{q}{\Delta T} = \frac{8609}{8} = 1076 \text{ J/kg. K}$$

This result matches the value of c_p (specific heat capacity when heat is supplied (removed) at constant pressure $(p = \text{const})\bar{c} = c_p$)

Using the Meyer formula (2.25), the specific heat capacity at constant volume can also be determined:

$$c_v = c_p - R = 1076 - 287.05 = 788.95 J/kg.K$$

Like As a consequence of this, the adiabatic coefficient is also calculatedx:

$$\varkappa = \frac{c_p}{c_n} = \frac{1076}{788.95} \approx 1.36$$

This value corresponds with high accuracy to the theoretical value for air ($\varkappa \approx 1.4$), which confirms the precision of the experiment.

To determine the molar specific heat capacity, the molecular mass (formula 2.27) of air is used $\mu=28.96$ kg/kmol:

$$c_M = \bar{c}.\mu = 1076.28.96 = 31.161 \text{ J/kmol}.K,$$

and based on this, the volumetric capacity, taking into account that vM = 22.4 m3/kmol is the gas volume under normal conditions according to formula (2.28):

$$c' = \frac{c_M}{v_M} = \frac{31161}{22.4} = 1391.11 \text{ J/m}^3.\text{K}.$$

The amendment of the enthalpy in an isobaric process is determined by (formula 2.29):

$$\Delta h = cp \cdot \Delta T = 1076 * 8 = 8 608 \text{J/kg}$$

And the corresponding change in internal energy in an isochoric process is (formula 2.32):

$$\Delta u = cv \cdot \Delta T = 788.95 .8 = 6311.6 \text{ J/kg}$$

We calculate the change in entropy using the following formula (2.35):

$$\Delta s = cpln \frac{T_2}{T_4} = 1076 \cdot ln \frac{307.75}{299.75} = 1076 \cdot 0.02526 = 27.17 \text{J/kg. K}$$

The absolute enthalpy relative to standard conditions (formula 2.31):

$$h2 = cp$$
. $(T3 - Tn) = 1076$. $(307.75 - 273.15) = 37 229$ J/kg

Internal energy (formula 2.34):

$$u2 = cv (T3 - TH) = 788.95 \cdot (307.75 - 273.15) = 27,297 \text{ J/kg}$$

In a similar way, the values at different frequencies of the asynchronous electric motor in the dissertation were calculated.

4.2.2 Results of analytical calculations

 Table 4.9
 Results of measured parameters at different frequencies

	Frequency	ρ	T_3	T_4	ΔT	v_5	Q	m
dim./ No.	Hz	kg/m^3	•C	•C	K	m/s	W	kg/s
1.	20	1.19	34.6	26.6	8.0	2.59	187.68	0.0218
2.	40	1.19	31.1	26.6	4.5	5.34	187.58	0.0432
3.	60	1.19	29.8	26.7	3.1	7.88	187.32	0.0630
4.	80	1.19	29.1	26.9	2.2	10.13	185.15	0.0805

Table 4.10 Results of measured heat capacities at different frequencies

	Frequency	\bar{c},c_p	c_M	c′	c_v
dim ./No	Hz	$J/\mathrm{kg}.K$	J/kmol.K	J/m ³ .K	J/kg.K
1.	20	1076	31161	1391.11	788.95
2.	40	964.88	27942	1247.41	677.83
3.	60	959.03	27773	1239.86	671.98
4.	80	1044	30234	1349.73	756.95

 Table 4.11
 Results of measured thermodynamic parameters

	Frequency	Δh	h2	∆you	<i>u</i> 2	Δs
dim ./No	Hz	J/kg	J/kg	J/kg	J/kg	J/kg. K
1.	20	8608	37229	6311.6	27297	27.17
2.	40	4342	30007	3050.24	21080	14.35
3.	60	2972	28579	2083.14	20025	9.78
4.	80	2296	30380	1665.3	22027	7.51

4.3 CONCLUSIONS UNDER CHAPTER 4

Based on the results obtained in the fourth chapter, it can be concluded that the developed automated laboratory system with remote access successfully fulfills the objectives of the study and confirms its functionality and reliability in experimental determination of aerodynamic and thermodynamic parameters of the air flow. The conducted experiments demonstrate correspondence between the theoretical models and real measurements, which validates the developed methodologies and their practical application.

The obtained relationships between velocity, volumetric and mass air flow rates show a high degree of correlation ($R^2 = 0.999$), proving the accuracy and stability of the measurement system.

CHAPTER 5. CONCLUSIONS AND CONTRIBUTIONS OF THE DISSERTATION

Scientific and applied contributions:

- 1. Developed and adapted for the specifics of remote sensing in real-time operation is a methodology for measuring the air flow velocity profile, based on a Pitot tube and a differential pressure sensor. It provides high precision and reliability of the results. The integration of the velocity profile allows for accurate calculation of the air flow rate, which is essential for educational and engineering applications;
- 2. Developed and adapted for the specifics of remote sensing in real-time operation is a methodology for measuring the specific heat capacity of air at constant pressure. It is based on determining the mass flow rate of air in a pipe channel and measuring the heat transfer rate from a heating element and the temperature difference in the flow before and after the heater. The methodology also takes into account the current value of the atmospheric pressure in the measurement area, which affects the air density. In addition to the specific heat capacity, a number of other thermodynamic parameters of the air are determined in the heat exchange process;
- 3. An approach for remote activation and control of stands and servers has been developed and tested, based on the Modbus over TCP/IP protocol, in combination with Remote Desktop remote access to the server by the teacher and granting access rights to the student, through popular videoconferencing platforms such as Microsoft Teams, Google Meet, or Zoom. This approach provides remote activation of both the teacher and the student and allows for monitoring and control by the teacher, as well as possible intervention at any time. In this case, only standard applications are used and the need to develop a specialized website is avoided.

Applied contributions:

- 1. Based on an existing stand, model SR1162E, the hardware and software of a modernized laboratory stand have been designed and tested, providing the possibility of remote access and control, and having a modular and scalable architecture, with the ability to implement complex measurement and control tasks, through a centralized microcontroller system. A number of measurement and executive modules have been added to the stand, which have a digital interface based on RS485 over ModBus protocol. The choice of microcontroller STM32F103ZE is justified by comparison with alternatives (ESP32, Arduino Mega), as it offers the best balance between computing power, communication interfaces and hardware reliability for the purposes of remote control and data collection;
- 2. A communication controller has been developed a basic element in the construction of the automated system, as it acts as an interface between the physical measuring/executive devices and the application software (server) implemented in Node-RED. The controller is implemented on a platform with an embedded STM32 microcontroller, functioning as an embedded PLC. It collects data from various peripheral modules via the industrial serial protocol Modbus RTU and transmits them to the HMI interface implemented in Node-RED. In addition, the communication

- controller is responsible for transmitting control commands back to the actuators.
- 3. In Node-RED, an application server is designed, which is installed on a personal computer (server). It implements a logical connection with the task of communication between the hardware part (the microcontroller of the stand) and the external interface and performs several key functions. Along with visualization and control, Node-RED also performs logical operations, including comparison of values, mathematical calculations, data transformations, decision making and generation of control signals depending on the incoming input information.
- 4. An experimental validation of the functioning of the stand in remote mode was carried out. With its help, the developed adapted methodologies for measuring the air flow velocity profile and measuring the specific heat capacity of air at constant pressure were also validated. The measurements and analyses of the obtained data prove its applicability both in educational and research aspects, thanks to its flexible architecture, reliable communication mechanisms and capabilities for remote access and automation;
- 5. Two sets of methodological instructions have been developed for students: for measuring the air flow velocity profile and for measuring the specific heat capacity of air at constant pressure.

LIST OF PUBLICATIONS RELATED TO THE DISSERTATION

- 1. R. Popov, A. Parushev, A. Chekichev and N. Paunkov, "Remote Monitoring of the Atmosphere Air Quality," 2024 XXXIII International Scientific Conference Electronics (ET), Sozopol, Bulgaria, 2024, pp. 1-5, doi: 10.1109/ET63133.2024.10721563. (Scopus).
- 2. **A. Parushev**, A. Chekichev, S. Lyubomirov, R. Popov, N. Paunkov. VIRTUAL BENCH FOR REMOTE MEASUREMENT OF AIR FLOW VELOCITY IN A DUCT THROUGH A PIT TUBE, INTED 2023 17th annual International Technology Education and Development Conference Valencia (Spain) -6th, 7th and 8th of March, 2023 (online), Pages: 5536-5541, ISBN: 978-84-09-49026-4. doi:10.21125/inted.2023.
- 3. **Parushev**, A. Chekichev, N. Paunkov, R. Popov, S. Lyubomirov. VIRTUAL BENCH FOR REMOTE MEASUREMENT OF THE SPECIFIC HEAT CAPACITY OF AIR, INTED 2023 17th annual International Technology Education and Development Conference Valencia (Spain) -6th, 7th and 8th of March, 2023 (online), Pages: 5248-5253, ISBN: 978-84-09-49026-4. doi:10.21125/inted.2023.
- 4. **A. Parushev**, A. Chekichev, R. Popov. BUILDING A VIRTUAL LABORATORY BENCH TO EXAMINE HEAT TRANSFER PROCESSES,ICERI 2022 15th annual International Conference of Education, Research and Innovation (online), Pages: 4760-4764 ISBN: 978-84-09-45476-1. DOI:10.21125/iceri.2022.
- 5. A. Cekichev, A. Parushev, R. Popov. BUILDING A VIRTUAL INSTRUMENT FOR RESEARCH AND ANALYZING FILTERS IN LABVIEW AND MATLAB, ICERI 2022 15th annual International Conference of Education, Research and Innovation (online), Pages: 4795-4800 ISBN: 978-84-09-45476-1. DOI: 10.21125/iceri.2022.
- 6. N. Paunkov, R. Popov, A. Chekichev, A. Parushev, S. Lyubomirov. MAGNETIC FIELD MEASUREMENT WITH MICROPROCESSOR PLATFORM WITH INTELLIGENT SENSOR, INTED 2023 17th annual International Technology Education and Development Conference Valencia (Spain) -6th, 7th and 8th of March, 2023 (online), Pages: 5282-5289, ISBN: 978-84-09-49026-4. doi:10.21125/inted.2023.